frontiers | Frontiers in Physics

TYPE Original Research
PUBLISHED 08 January 2025
DOI 10.3389/fphy.2024.1461255

OPEN ACCESS

EDITED BY
Zhen Cheng,
Chinese Academy of Sciences (CAS), China

REVIEWED BY
Francesco Faita,
Institute of Clinical Physiology, Italy
Imran Iqbal,
New York University, United States

*CORRESPONDENCE
Michael Figl,
michael.figl@muv.ac.at

RECEIVED 08 July 2024
ACCEPTED 13 December 2024
PUBLISHED 08 January 2025

CITATION
Zalka L, Köhrer J, Songsaeng C, Homolka P, Kollmann C, Hummel J and Figl M (2025) Application of additive manufacturing for the adaptive design of ultrasound phantoms. *Front. Phys.* 12:1461255. doi: 10.3389/fphy.2024.1461255

Application of additive manufacturing for the adaptive design of ultrasound phantoms

Lukas Zalka[1,2], Johannes Köhrer[1,2], Chatsuda Songsaeng[1,2], Peter Homolka[1], Christian Kollmann[1], Johann Hummel[1,2] and Michael Figl[1,2]*

[1]Center for Medical Physics and Biomedical Engineering, Medical University of Vienna, Vienna, Austria, [2]Christian Doppler Laboratory for Mathematical Modelling and Simulation of Next-Generation Medical Ultrasound Devices, Medical University of Vienna, Vienna, Austria

Introduction: The image formation process of conventional pulse-echo Ultrasound mainly uses the backscattered amplitude and assumes constant attenuation and speed of sound in the penetrated media. Thus, many commercially available ultrasound imaging phantoms use only a limited choice of materials with simple geometric shapes. Part of today's research in ultrasound is to gain more information on the acoustic properties of the object imaged. These advanced imaging and reconstruction procedures require more complicated phantom designs that contain different materials with precisely designable acoustic properties for validation and quality assurance (QA).

Methods: To fabricate such phantoms, we produced molds for casting ultrasound phantoms using additive manufacturing. Phantom materials used were based on agar and polyvinyl alcohol. To adapt the speed of sound glycerol was added to the mixtures. As glycerol diffuses out of the phantom material, polluting the surrounding water, we designed a watertight sample holder. The effect of the freeze-thaw cycles (FTCs) on the acoustic properties of the polyvinyl alcohol (PVA)-based phantoms was also investigated. Speed of sound and attenuation were determined for both phantoms materials, and Shore hardness measured for the PVA-based phantoms.

Results: Shore hardness of the PVA phantoms increased by up to 79% of the initial value with increasing number of freeze-thaw cycles, but showed a saturation after 5 FTCs. However, the number of FTCs had only a small effect on the speed of sound and attenuation, as the sound speed increased slightly from 1,530.14 m/s to 1,558.53 m/s, (1.86%) and the attenuation exhibited only an increase of 6.75%. In contrast, differences of around 100 m/s in the speed of sound in the PVA phantoms (from 1,558.53 to 1,662.27 m/s), as well as in the agar-based phantoms (from 1,501.74 to 1,609.36 m/s) could be achieved by adding glycerol, making these materials appropriate candidates for the design and fabrication of US phantoms with defined sections and details with different speed of sound and attenuation. The use of the sample holder showed only an influence of 0.63% on the measured speed of sound.

Discussion: 3D printed molds led to an improved manufacturing process as well as a free choice of the shape of the phantoms. A sample holder could prevent

contamination of the water with no significant differences in the measured speed of sound.

KEYWORDS

ultrasound phantom, speed of sound, attenuation, additive manufacturing, polyvinyl alcohol, agar

1 Introduction

The image formation process of conventional pulse-echo Ultrasound uses mainly the backscattered amplitude [1, 2]. An important assumption for image reconstruction is that attenuation and speed of sound are constant in the penetrated media. Thus, many commercially available ultrasound imaging phantoms used for quality assurance (QA) or performance evaluation consist of a limited choice of materials, e.g., scattering objects embedded in a background material, for example, the 3D calibration phantom ATS560 [3]. However, backscatter is caused by the differences in impedance and, as densities for soft tissues are quite similar, mainly by differences in the speed of sound [1, 4]. Quantitative reconstruction of acoustic properties, like attenuation or sound velocity, has a wide variety of applications from breast imaging to liver fat quantification [5–8]. Such imaging procedures require more complicated phantom designs containing different materials with precisely known acoustic properties for validation and QA [9–12]. Modern ultrasound image formation and reconstruction algorithms have a great potential for highly specific applications in particular body regions [13]. The design of phantoms using materials and shapes that can be adapted to the applications and development stages of these algorithms is paramount for their validation.

An interesting field of application for custom-made imaging phantoms opens up with the advent of AI methods in medical image analysis with applications in almost every medical field [14–19]. In a recent editorial, the issue of accountability of AI tools was connected to the black box effect AI methods often have, [20]. Imaging phantoms tailored to their particular areas of application are therefore expected to contribute to an improved understanding of how the AI systems come to their conclusions.

Using polyvinyl alcohol (PVA) based phantom material from [21] and additively manufactured molds, we produced Ultrasound phantoms in simple shapes. PVA-based materials need several freeze-thaw cycles (FTC) to form a gel network and increase the strength of the material, see [22, 12]. The gelation process was monitored by Shore hardness measurements.

Additionally, agar-based phantoms were made according to the recipe of [23]. Agar is a commonly used material for ultrasound phantoms, see, e.g., [24–26], and is used here because of its simple production process.

Basic properties of these phantoms were measured using a simple, specially developed measurement setup. Such a basic evaluation of, e.g., speed of sound is supposed to be performed prior to the usage of the phantoms, as their acoustical properties might change with time and cannot be assured with the accuracy necessary for the evaluation of reconstruction algorithms otherwise [12]. Additively manufactured phantom mounts were developed and used to avoid pollution of the measurement setup by the phantom material.

2 Materials and methods

2.1 Phantom design

2.1.1 Phantom material

The PVA-based phantoms were made using > 99%+ hydrolyzed PVA with a molar mass of 85,000-140,000 g/mol (Sigma-Aldrich, St. Louis, MO, United States) and deionized water (DI water) to obtain a 10% PVA solution. Methylparaben (Methyl-4-hydroxybenzoate, Sigma-Aldrich, St. Louis, MO, United States) was added to reduce degradation by bacteria and fungi. A slightly altered additional phantom was based on the material as above adding glycerol (Sigma-Aldrich, St. Louis, MO, United States) to increase the speed of sound.

The same additives were used for the agar-based phantoms. However, as base material, instead of PVA agar (E406, Biomus, Lublin, PL) with a gelation power of 900 g/cm^2 was used. The ingredients of the phantom materials can be found in Table 1.

2.1.2 Phantom mold design

After mixing in a water bath under controlled temperature, the still hot viscous phantom material was transferred into the 3D printed molds for gelation. To design the molds, Fusion 360 (Autodesk, San Francisco, CA, United States, software version 2.0.16985) was used. We printed the molds with an Ultimaker 2 Fused Deposition Modeling (FDM) printer, (Ultimaker, Geldermalsen, NL) with polylactic acid (ecoPLA Tough, 3D Jake, Paldau, AT) as filament material. For uniform freezing of the PVA we allowed air circulation by adding spaces between the chambers of the mold, see Figure 1. Covers were printed to close the chambers and prevent the evaporation of water from the material.

For measurement, it is often necessary to submerge the phantoms in water for a considerable amount of time. Phantom base material not perfectly polymerized or added substances like glycerol might then dissolve from the phantom material, contaminating the water and modify the proportion of, e.g., PVA to Glycerol in the phantom. This results in compromising measurements by changing both, water and phantom parameters. A setup was developed that prevents direct contact between water and the phantom, see Figure 2. This setup resembles a drum and consists of four rings, a tube, and 25 µm thick Saran Wrap© (Extol, OH, United States). The individual parts were also designed in Fusion 360 and printed using the Form 3B + printer and the Clear resin V4, from Formalbs (Formlabs, MA,United States). Due to the drum-like structure, the Saran foil can be stretched to prevent wrinkles. Additionally, the construction can be assembled underwater and therefore no air is trapped between the phantom and the foil. This design also allows the use of liquid and semi-solid phantom materials.

10.3389/fphy.2024.1461255

TABLE 1 The ingredients of the phantom materials.

PVA phantoms	PVA [g]	Methylparaben [g]	DI water [g]	Glycerol [g]
PVA	30	0.8	269.2	0
PVA + Glycerol (18%)	70	1.4	502.6	126
Agar phantoms	**Agar [g]**	**Methylparaben [g]**	**DI water [g]**	**Glycerol [g]**
Agar	9	1.38	289.62	0
Agar + Glycerol (5%)	6	0.92	183.08	10
Agar + Glycerol (11.2%)	9	1.38	255.99	33.63
Agar + Glycerol (15%)	9	1.38	244.62	45
Agar + Glycerol (20%)	9	1.38	229.62	60

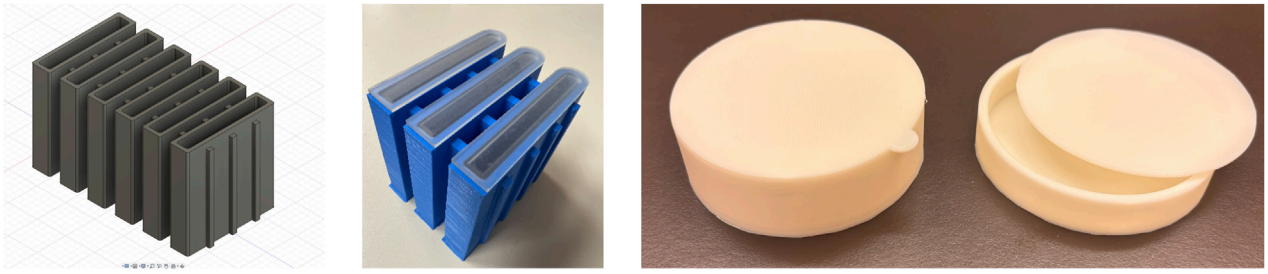

FIGURE 1
Model and finished 3D printed molds for the phantom materials.

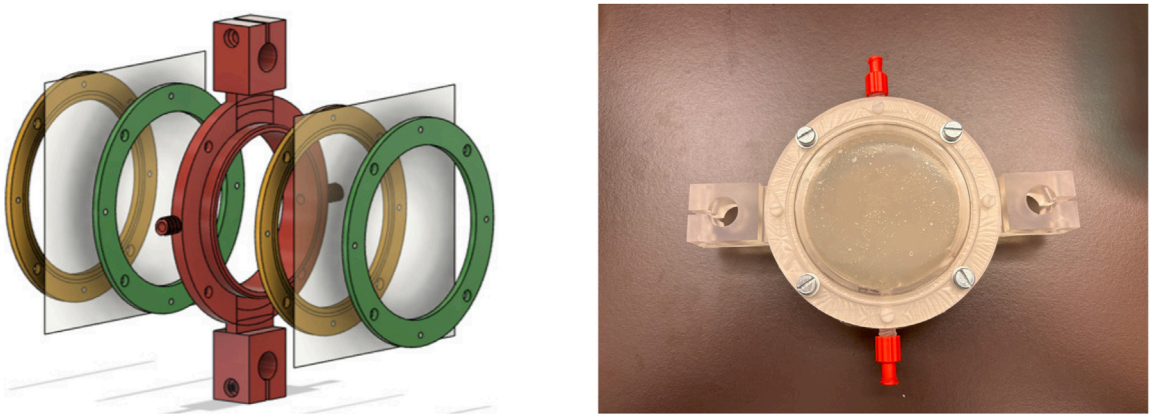

FIGURE 2
Model and setup to avoid contact of water and phantom.

2.1.3 Preparation of the PVA base material

For the PVA cryogel we used 30 g PVA powder and 0.8 g Methylparaben. Both substances were dissolved in 269.2 g of DI water at 23.2°C. The solution was mixed for 60 min at 253 rpm and heated up to 85°C, the temperature was measured every 10 minutes. Evaporation was monitored by weighing the solution before and after mixing. The water lost due to evaporation was replenished after mixing to obtain the concentrations intended. The solution was then kept at 85°C for 60 min for degassing of the PVA. Air bubbles were removed by skimming the surface of the mixture with a metal blade.

After cooling down to 23.0°C the mixture was poured into the molds. The molds were then sealed with plastic lids to avoid further

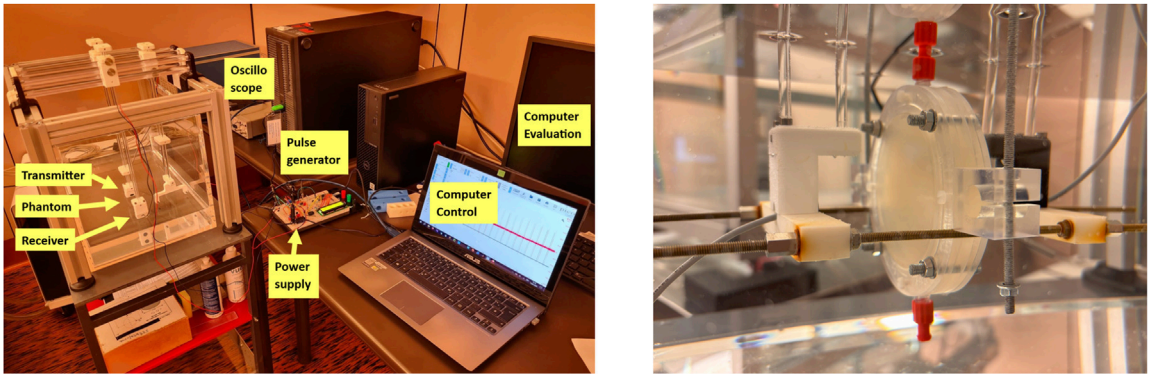

FIGURE 3
Left: overview of the measurement setup, right: alignment setup for transmitter, phantom sample holder and receiver.

TABLE 2 Sound velocity of PVA phantom material versus numbers of FTCs.

Freeze/thaw cycles	Speed of sound [m/s]
1	1,530.14 ± 9.85
2	1,533.93 ± 4.88
3	1,538.81 ± 1.32
10	1,558.53 ± 6.09

TABLE 3 Speed of sound of PVA + Glycerol material after storage in containers filled with DI water or with DI water with 18% Glycerol.

Storage	Speed of sound [m/s]
in DI water	1,570.29 ± 2.14
in 18% Glycerol	1,662.27 ± 8.35

evaporation of water and put in a freezer at −20°C. For initiating the gelation process, 8 h freezing were followed by 16 h thawing at 6°C in the refrigerator. Up to ten FTCs were applied consecutively. Afterwards, the phantoms were removed from the molds and stored in a plastic container filled with DI water.

For the phantom material containing PVA and glycerol we applied the same process with the appropriate amount of glycerol added into the liquid phase. We used 70 g PVA powder, 1.4 g Methylparaben, 502.6 g DI water and 126 g glycerol resulting in a 10% PVA hydro-cryogel with 18% glycerol w/w.

2.1.4 Preparation of the agar based phantom materials

To prepare the agar phantoms, also methyl-4-hydroxybenzoate was added to reduce bacterial and fungal decay. After mixing, the solution was placed in an oven preheated to 90°C and heated for 4 h. Then, the mixture was removed from the oven and weighed again to determine how much water had evaporated during the heating process. The missing weight was compensated for with DI water. The mixture was allowed to cool to 50°C and was then poured into the prepared containers. Finally, the foam that had formed on the surface of the material was removed and the mixture was cooled to room temperature (22°C). In addition, agar-based phantoms were prepared with glycerol to change their physical properties. The quantities of the individual ingredients are shown in Table 1.

2.2 Measurements of acoustical properties

2.2.1 Measurement set up for speed of sound and attenuation

For the measurement of the speed of sound and attenuation we used the transmission principle as described in the AIUM standard [27]. In our setup, the transmitter and receiver consisted of single-element liquid flow sensors (US0072 and US0075, Audiowell Electronics Zhaoqing, China). These sensors emit an ultrasonic wave with 1 MHz center frequency. The transmitter was controlled using a Teensy 4.0 microcontroller (PJRC.COM, LLC., 14,723 SW Brooke CT Sherwood, OR 97140 United States). The received signals were acquired by an oscilloscope (Picoscope 5244D, Pico Technology, Steinfurt, DE), and the data is processed with MATLAB (R2023a; Mathworks, Natick, MA, United States). For measurements the mount and the fastening parts are placed in a water tank filled with DI water. Because the speed of sound is temperature dependent, see [28], the temperature in the water tank is constantly monitored during a series of measurements using a thermometer. The setup also included a construction that aligns the sensors and the phantom to each other, see Figure 3.

2.2.1.1 Speed of sound

In the above described transmission setup, the speed of sound is measured using the substitution method. During a first measurement, the sound wave travels from transmitter to receiver without a phantom. In a second measurement, the phantom to be measured is placed between the two sensors. The difference in arrival time Δt can be used to determine the speed of sound c_p in the material, given its thickness d and the speed of sound c_w in water. For both measurements, without and with phantom

in place, five pulses were read into MATLAB and a band pass filter (900 kHz–1.1 Mhz) applied and an envelope placed over the averaged pulses using the Hilbert transform. The maxima of the envelopes define the arrival times of the measurements determining their difference Δt. The speed of sound in the phantom is determined according to Formula 1

$$c_p = \frac{c_w}{1 + \Delta t \frac{c_w}{d}}. \quad (1)$$

2.2.1.2 Attenuation

The attenuation coefficient of the phantom is also determined using the substitution method using the amplitudes of the arrived pulses. Also, measurements of five pulses were averaged. The amplitude values of the maxima A_0 without phantom and A_p with the phantom are compared in Formula 2 for the calculation of the attenuation, where T is the amplitude transmission coefficient from water to the phantom material, and d the material thickness, respectively.

$$\alpha = \frac{20}{d} \log_{10} \frac{A_0 \cdot T^2}{A_p} \quad (2)$$

2.2.2 Shore hardness

To determine when there is no further progress in the gelation process, Shore hardness of the PVA phantoms was measured using a durometer (HPE II, Bareiss GmbH, Baiersbronn, Germany) applying the Shore 000s hardness scale. The measurements were carried out in accordance with the guideline D2240-15 of [29]. Care was taken to ensure that the measuring points were not too close to the edges of the phantoms, as this could result in incorrectly measured values. A minimum distance of 10 mm was left to the edges. A total of 10 measurements were obtained for each phantom and averaged. In order to determine the effect of the number of FTCs on the hardness of the phantoms, three PVA phantoms were measured after each of 10 subsequent FTCs.

3 Results

3.1 Speed of sound

3.1.1 Speed of sound in PVA depending on the FTCs

The measured speed of sound for phantom material PVA, which underwent a different number of FTCs, can be found in Table 2. The values shown were determined from three PVA phantoms, each of which was subjected to 1, 2, 3 and 10 FTCs, consecutively. The temperature of the phantoms was 23.5 ± 0.2°C, the surrounding water had a temperature of 21.8 ± 0.1°C.

The measured speed of sound of the PVA phantoms containing glycerol can be seen below in Table 3. Two phantoms went through ten FTCs and were stored in DI water, whereas three phantoms went through three FTCs and were stored in a container with DI water with the same concentration of glycerol added as used for the phantom material. During the measurement the temperature of the phantoms was 23.4 ± 0.2°C and the water in the tank had a temperature of 22.9 ± 0.2°C. A significant difference in sound speed in the two columns of Table 3 was found (t-test, $p < 0.01$).

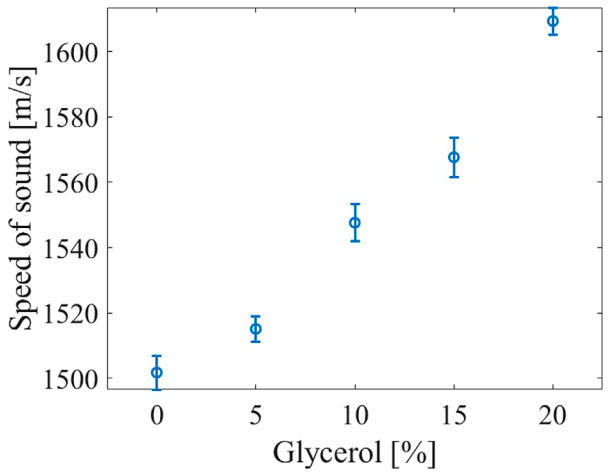

FIGURE 4
The effect of glycerol on the speed of sound in agar-based phantoms.

TABLE 4 The effect of glycerol on the speed of sound in agar-based phantoms.

Material	Speed of sound [m/s]
Agar	1,501.73 ± 4.24
Agar + Glycerol (5%)	1,515.08 ± 3.13
Agar + Glycerol (10%)	1,547.60 ± 4.69
Agar + Glycerol (15%)	1,567.66 ± 4.90
Agar + Glycerol (20%)	1,609.36 ± 3.38

TABLE 5 Attenuation coefficient of a PVA phantoms with 3 and 10 FTCs and for the Agar-Glycerol (20%) phantom.

Phantom material	Attenuation coefficient [dB/(cm·MHz)]
Agar + Glycerol (20%)	0.3711 ± 0.043
PVA, 3 FTCs	0.7579 ± 0.0685
PVA, 10 FTCs	0.8091 ± 0.0184

For the Agar based phantoms the effect of glycerol on the speed of sound was measured. The phantoms had a temperature of 19.72 ± 1.21°C, the temperature of the surrounding water was 20.91°C during the measurement. The determined sound speeds can be seen in Figure 4 and Table 4.

To investigate the influence of the phantom sample holder (see Figure 3) on the speed of sound of an Agar + Glycerol (20%) phantom we measured three times without the device and with the device. The water temperature during the measurement was 22.3°C and the temperature of the phantoms was 20.1°C. The results of the sound speed of the phantoms showed a 0.63% difference if the phantom was sealed in the construction.

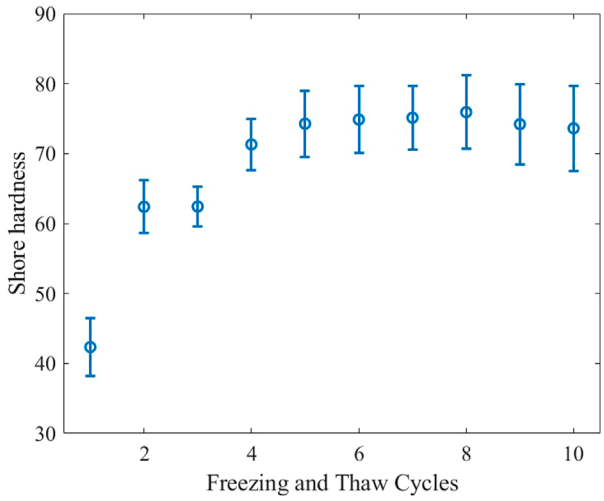

FIGURE 5
Progression of the Shore hardness of PVA based phantoms over the course of 10 FTC.

TABLE 6 Progression of the Shore hardness of PVA based phantoms over the course of 10 FTC.

FTCs	Shore hardness [%]
1	42.3 ± 4.1
2	62.4 ± 3.8
3	62.4 ± 2.8
4	71.3 ± 3.6
5	74.3 ± 4.7
6	74.9 ± 4.8
7	75.1 ± 4.6
8	75.9 ± 5.3
9	74.2 ± 5.7
10	73.6 ± 6.1

3.2 Attenuation

The attenuation coefficient was measured for Agar + Glycerol (20%) and for PVA with 3 and 10 FTCs. The temperature of the water during the measurement was 22.3°C and the temperature of phantom material was 22.3°. The numbers can be found in Table 5.

3.3 Shore hardness

To determine the plateau where no further or only minimal material changes occur with additional FTCs we measured the Shore hardness of three PVA phantoms after each of 10 consecutive FTCs, see Figure 5 and Table 6.

4 Discussion

We produced 3D printed molds for ultrasound phantom materials and used a simple setup to measure their acoustical properties. Such a setup should be supportive in demand-oriented phantom design as some ultrasound phantoms materials might change their acoustical properties as a consequence of storage or aging [12]. We could see this effect clearly for the PVA + Glycerol phantoms, see Table 3 where the phantom stored in DI water leaked glycerol from diffusion into the storage solution, resulting in a reduction of the speed of sound measured. For evaluation of novel innovative US imaging and reconstruction algorithms, or in the emerging field of AI methods, but also in quality assurance, it might be more appropriate or even necessary to produce phantoms from a pre-fabricated material on demand and then measure elementary acoustical properties immediately before use. On the other hand, appropriate storage (in the case of PVA + Glycerol material in a Glycerol solution) or suitable design might ensure long time stability of parameters [30, 31].

For PVA based phantoms the speed of sound slightly increased with the number of FTCs, see Table 2. This might be due to the fact that the PVA chains become longer with each FTC, which also increases the density of the phantom, resulting in a higher speed of sound. In [21] a similar effect is described for the first three FTCs, but like in our data with overlapping standard deviations of the measurements, no uniform effect was found in [32].

Phantoms made from PVA with added glycerol, and the series of agar phantoms with increasing amounts of glycerol, showed that the speed of sound can be increased with the addition of glycerol. This results align with of [33].

It could be observed that the phantoms begin to shrink and thus lose thickness visibly after four to five FTCs (see Figure 6). This was also evident in the measurement of Shore hardness. The phantoms exhibited an increase in hardness with FTCs, which leveled off to approach a plateau after the fifth FTC (see Figure 5).

Furthermore, previous tests have shown that storage during the FTCs affects the phantom material as well as medium in which it is stored or emersed. It was found that the glycerol tends to diffuse out of the phantom material into the surrounding water if stored in a solution without glycerol added, like pure DI water. In the containers in which the phantoms were stored as well as in the water tank in which they were measured, PVA threads and impurities were found. For the PVA + Glycerol phantoms this could be observed when comparing speed of sound for the phantoms stored in a glycerol solution to the values measured with those phantoms, which were stored in DI water, see Table 3.

Additionally, this effect can be seen in the measurement with and without the sample material holder being used to accommodate the phantom. There, the speed of sound of the Agar + Glycerol (20%) phantom is in both cases lower than in earlier measurements with the same material (see Figure 4; Table 7).

Phantom measurements for testing purposes are typically performed in a hydrophone scanning system (e.g., the Acoustic Intensity Measurement System (AIMS) by ONDA (ONDA Corporation, Sunnyvale, CA, United States) [34]) with a much

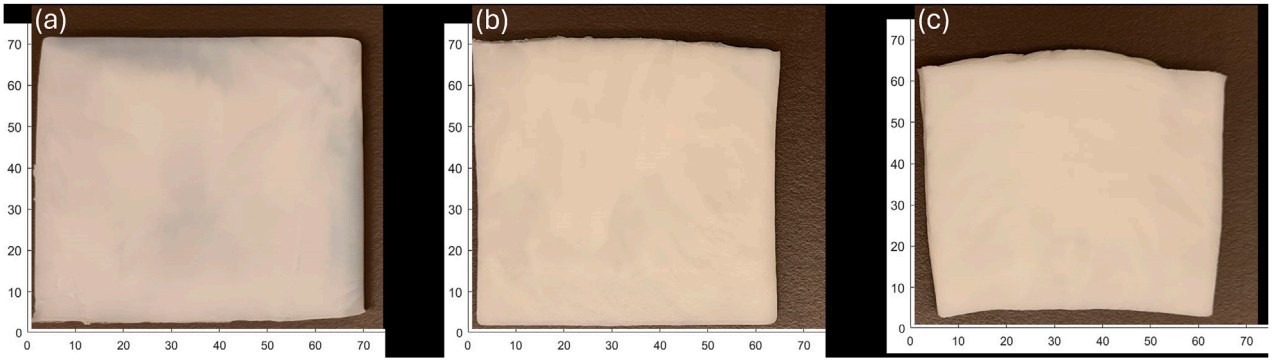

FIGURE 6
One of the PVA phantoms after three **(A)**, five **(B)** and ten **(C)** FTCs. Shrinkage and deformation of phantoms can be seen over the course of the freezing cycles.

TABLE 7 Comparison of speed of sound, where a Agar + Glycerol (20%) was measured with and without the measuring construction.

	Speed of sound [m/s]
without sample holder	1,588.57 ± 5.04
with sample holder	1,578.52 ± 1.88

bigger tank, where the water quality is important for the hydrophone. To avoid pollution of the tank and the sensitive measurement equipment, a protective cover shielding the phantom material from the surrounding water similar to the one shown in Figure 2 could be helpful. The influence of the sample holder was negligible, which is in accordance with a comparable result in [11].

The determination of the attenuation coefficient with the simple setup from Figure 3 proved to be challenging. The fluctuations in the signal amplitude, probably caused by considerable noise from the amplifier circuit, needed additional filtering in software to stabilize the results.

An additional calibration procedure comparing the results to those of standardized materials with well known and tabulated properties, and more elaborate measurement equipment with a calibrated hydrophone would be desirable.

5 Conclusion

The 3D printed molds led to an improved manufacturing process as well as a free choice of the shape of the phantoms. As phantom materials can change in their acoustical properties during storage, a cheap and easy-to-use evaluation setup like the one presented in Figure 3 is helpful to re-check these properties before actual measurements or QC procedures.

Applying a sample holder as shown, contamination of the water can be prevented, allowing more accurate and reliable measurements. The use of this construction showed no significant differences in the measurement results, as speed of sound (see Table 7).

Data availability statement

The raw data supporting the conclusions of this article will be made available by the authors, without undue reservation.

Author contributions

LZ: Software, Writing–original draft. JK: Methodology, Writing–review and editing. CS: Methodology, Writing–review and editing. PH: Supervision, Writing–review and editing. CK: Data curation, Supervision, Writing–review and editing. JH: Data curation, Project administration, Supervision, Writing–review and editing. MF: Conceptualization, Funding acquisition, Methodology, Project administration, Resources, Supervision, Writing–review and editing.

Funding

The author(s) declare that financial support was received for the research, authorship, and/or publication of this article. This work was supported by the Austrian Research Promoting Agency (FFG) grants No. 861552 and No. 888047. Part of this research was supported by the M3dRES project infrastructure (Grant No. 858060), FFG. The financial support by the Austrian Federal Ministry for Digital and Economic Affairs, the National Foundation for Research, Technology and Development and the Christian Doppler Research Association is gratefully acknowledged.

Conflict of interest

The authors declare that the research was conducted in the absence of any commercial or financial relationships that could be construed as a potential conflict of interest.

The author(s) declared that they were an editorial board member of Frontiers, at the time of submission. This had no impact on the peer review process and the final decision.

Publisher's note

References

1. Flower M, editor. *Webb's physics of medical imaging*. Boca Raton: CRC Press (2012).

2. Samei E, Peck DJ. *Hendee's physics of medical imaging*. Wiley Blackwell (2019).

3. CIRS Inc. (2022) 3D calibration phantom ATS 560

4. Mast TD. Empirical relationships between acoustic parameters in human soft tissues. *Acoust Res Lett Online-arlo* (2000) 1:37–42. doi:10.1121/1.1336896

5. Hollenhorst M, Hansen C, Hüttebräuker N, Schasse A, Heuser L, Ermert H, et al. Ultrasound computed tomography in breast imaging: first clinical results of a custom-made scanner. *Ultraschall Med* (2010) 31:604–9. doi:10.1055/s-0029-1245506

6. Nebeker J, Nelson TR. Imaging of sound speed using reflection ultrasound tomography. *J Ultrasound Med* (2012) 31:1389–404. doi:10.7863/jum.2012.31.9.1389

7. Ferraioli G, Roccarina D, Barr RG, Weintraub E. Intersystem and interoperator agreement of US attenuation coefficient for quantifying liver steatosis. *Radiology* (2024) 313:e240162. doi:10.1148/radiol.240162

8. Cloutier G, Destrempes F, Yu F, Tang A. Quantitative ultrasound imaging of soft biological tissues: a primer for radiologists and medical physicists. *Insights Imaging* (2021) 12:127. doi:10.1186/s13244-021-01071-w

9. CIRS Inc. (2011) Elasticity QA phantom model 049 and 049A

10. Al-Mutairi FF, Chung EM, Moran CM, Ramnarine KV. A novel elastography phantom prototype for assessment of ultrasound elastography imaging performance. *Ultrasound Med Biol* (2021) 47:2749–58. doi:10.1016/j.ultrasmedbio.2021.05.015

11. Browne J, Ramnarine K, Watson A, Hoskins P. Assessment of the acoustic properties of common tissue-mimicking test phantoms. *Ultrasound Med Biol* (2003) 29:1053–60. doi:10.1016/s0301-5629(03)00053-x

12. Culjat MO, Goldenberg D, Tewari P, Singh RS. A review of tissue substitutes for ultrasound imaging. *Ultrasound Med Biol* (2010) 36:861–73. doi:10.1016/j.ultrasmedbio.2010.02.012

13. Sultan SR, Alghamdi A, Abdeen R, Almutairi F. Evaluation of ultrasound point shear wave elastography reliability in an elasticity phantom. *Ultrasonography* (2022) 41:291–7. doi:10.14366/usg.21114

14. Carrilero-Mardones M, Parras-Jurado M, Nogales A, Pérez-Martín J, Díez FJ. Deep learning for describing breast ultrasound images with BI-RADS terms. *J Imaging Inform Med* (2024) 37:2940–54. doi:10.1007/s10278-024-01155-1

15. Iqbal I, Younus M, Walayat K, Kakar MU, Ma J. Automated multi-class classification of skin lesions through deep convolutional neural network with dermoscopic images. *Comput Med Imaging Graphics* (2021) 88:101843. doi:10.1016/j.compmedimag.2020.101843

16. Iqbal I, Ullah I, Peng T, Wang W, Ma N. An end-to-end deep convolutional neural network-based data-driven fusion framework for identification of human induced pluripotent stem cell-derived endothelial cells in photomicrographs. *Eng Appl Artif Intelligence* (2025) 139:109573. doi:10.1016/j.engappai.2024.109573

17. Sundell V-M, Mäkelä T, Vitikainen A-M, Kaasalainen T. Convolutional neural network -based phantom image scoring for mammography quality control. *BMC Med Imaging* (2022) 22:216. doi:10.1186/s12880-022-00944-w

18. Qi Y, Guo Y, Wang Y. Image quality enhancement using a deep neural network for plane wave medical ultrasound imaging. *IEEE Trans Ultrason Ferroelectrics, Frequency Control* (2021) 68:926–34. doi:10.1109/tuffc.2020.3023154

19. Meng X, Ma J, Liu F, Chen Z, Zhang T. An interpretable breast ultrasound image classification algorithm based on convolutional neural network and transformer. *Mathematics* (2024) 12:2354. doi:10.3390/math12152354

20. Stefanini B, Giamperoli A, Terzi E, Piscaglia F. Artificial intelligence in ultrasound: pearls and pitfalls in 2024. *Ultraschall Med* (2024) 45:444–8. doi:10.1055/a-2368-9201

21. Sharma A, Marapureddy SG, Paul A, Bisht SR, Kakkar M, Thareja P, et al. Characterizing viscoelastic polyvinyl alcohol phantoms for ultrasound elastography. *Ultrasound Med Biol* (2023) 49:497–511. doi:10.1016/j.ultrasmedbio.2022.09.019

22. Adelnia H, Ensandoost R, Shebbrin Moonshi S, Gavgani JN, Vasafi EI, Ta HT. Freeze/thawed polyvinyl alcohol hydrogels: present, past and future. *Eur Polym J* (2022) 164:110974. doi:10.1016/j.eurpolymj.2021.110974

23. International Electrotechnical Commission. *Ultrasonics - real-time pulse-echo systems - test procedures to determine performance specifications*. American National Standards Institute (1996).

24. Teirlinck CJ, Bezemer RA, Kollmann C, Lubbers J, Hoskins PR, Ramnarine KV, et al. Development of an example flow test object and comparison of five of these test objects, constructed in various laboratories. *Ultrasonics* (1998) 36:653–60. doi:10.1016/s0041-624x(97)00150-9

25. Manickam K, Machireddy R, Seshadri S. Characterization of biomechanical properties of agar based tissue mimicking phantoms for ultrasound stiffness imaging techniques. *J Mech Behav Biomed Mater* (2014) 35:132–43. doi:10.1016/j.jmbbm.2014.03.017

26. Ramnarine KV, Anderson T, Hoskins PR. Construction and geometric stability of physiological flow rate wall-less stenosis phantoms. *Ultrasound Med Biol* (2001) 27:245–50. doi:10.1016/s0301-5629(00)00304-5

27. American Institute of Ultrasound in Medicine, and Technical Standards Committee (1995) *Methods for specifying acoustic Properties of tissue-mimicking Phantoms and objects* (American Institute of ultrasound in medicine)

28. Bilanuk N, Wong G. Speed of sound in pure water as a function of temperature. *J Acoust Soc Am* (1993) 93:1609–12. doi:10.1121/1.406819

29. American Society for Testing and Materials *Standard test method for rubber property - durometer hardness*, D2240-15. American Society for Testing and Materials (2021).

30. Taghizadeh S, Labuda C, Mobley J. Development of a tissue-mimicking phantom of the brain for ultrasonic studies. *Ultrasound Med Biol* (2018) 44:2813–20. doi:10.1016/j.ultrasmedbio.2018.08.012

31. Cabrelli LC, Pelissari PIBGB, Deana AM, Carneiro AAO, Pavan TZ. Stable phantom materials for ultrasound and optical imaging. *Phys Med Biol* (2016) 62:432–47. doi:10.1088/1361-6560/62/2/432

32. Elvira L, Durán C, Higuti RT, Tiago MM, Ibáñez A, Parrilla M, et al. Development and characterization of medical phantoms for ultrasound imaging based on customizable and mouldable polyvinyl alcohol cryogel–based materials and 3-d printing: application to high-frequency cranial ultrasonography in infants. *Ultrasound Med Biol* (2019) 45:2226–41. doi:10.1016/j.ultrasmedbio.2019.04.030

33. Cannon LM, Fagan AJ, Browne JE. Novel tissue mimicking materials for high frequency breast ultrasound phantoms. *Ultrasound Med Biol* (2011) 37:122–35. doi:10.1016/j.ultrasmedbio.2010.10.005

34. ONDA corp. (2020) Acoustic intensity measuring system